Interfacial characterization of ceramic core materials with veneering porcelain for all-ceramic bi-layered restorative systems*

Alexander Tagmatarchis, DDS, Dr Dent
Research Associate, Department of Biomaterials, University of Athens, School of Dentistry, Greece

Aris-Petros Tripodakis, DDS, MS, Dr Dent
Associate Professor, Department of Prosthodontics, University of Athens, School of Dentistry, Greece

Gerasimos Filippatos, DDS, MS
Clinical Instructor, Department of Prosthodontics, University of Athens, School of Dentistry, Greece

Spiros Zinelis, PhD
Assistant Professor, Department of Biomaterials, University of Athens, School of Dentistry, Greece

George Eliades, DDS, Dr Dent
Professor, Department of Biomaterials, University of Athens, School of Dentistry, Greece

* The paper was awarded the 1st prize of the 5th EAED Scientific Research Awards at the 26th EAED Annual meeting in Cesme Turkey 24–26 May 2012.

Correspondence to: Dr A Tagmatarchis
Konstantinoupoleos 12, 171 21 N. Smirni, Athens, Greece
Tel/Fax: +30 210 9523924; email: alex.tagma@yahoo.com

Abstract

Objective: The aim of the study was to characterize the elemental distribution at the interface between all-ceramic core and veneering porcelain materials.
Materials and methods: Three groups of all-ceramic cores were selected: A) Glass-ceramics (Cergo, IPS Empress, IPS Empress 2, e-max Press, Finesse); B) Glass-infiltrated ceramics (Celay Alumina, Celay Zirconia) and C) Densely sintered ceramics (Cercon, Procera Alumina, ZirCAD, Noritake Zirconia). The cores were combined with compatible veneering porcelains and three flat square test specimens were produced for each system. The core–veneer interfaces were examined by scanning electron microscopy and energy dispersive x-ray microanalysis.
Results: The glass-ceramic systems showed interfacial zones reach in Si and O, with the presence of K, Ca, Al in core and Ca, Ce, Na, Mg or Al in veneer material, depending on the system tested. IPS Empress and IPS Empress 2 demonstrated distinct transitional phases at the core–veneer interface. In the glass-infiltrated systems, intermixing of core (Ce, La) with veneer (Na, Si) elements occurred, whereas an abrupt drop of the core–veneer elemental concentration was documented at the interfaces of all densely sintered ceramics.
Significance: The results of the study provided no evidence of elemental interdiffusion at the core–veneer interfaces in densely sintered ceramics, which implies lack of primary chemical bonding. For the glass-containing systems (glass-ceramics and glass-infiltrated ceramics) interdiffusion of the glass-phase seems to play a critical role in establishing a primary bonding condition between ceramic core and veneering porcelain.

(Int J Esthet Dent 2014;9:536–550)

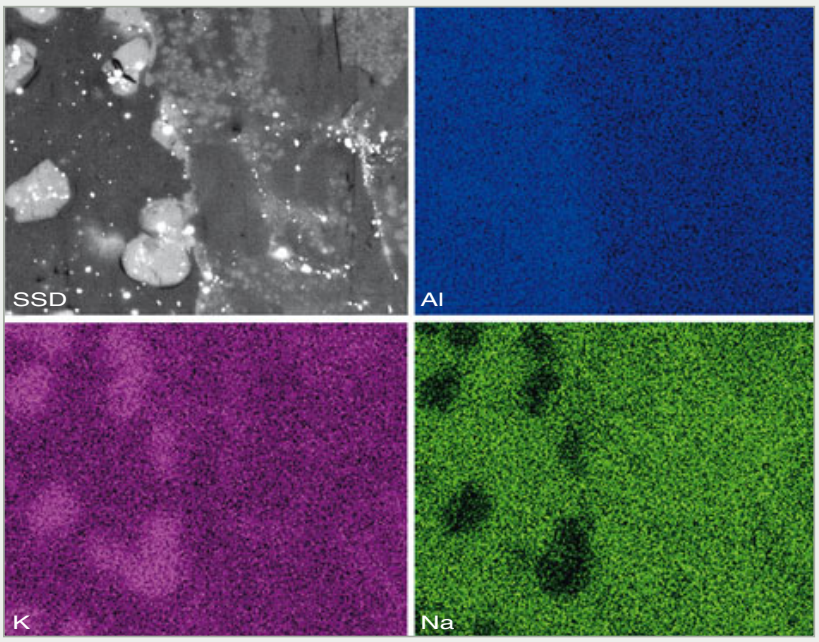

Introduction

The gold standard of the interfacial bond between the veneer ceramics and the supporting framework structures in fixed prosthodontics has been established over the years by the metal-ceramic restorations. The excellent wetting ability of silica-based feldspathic porcelain veneers upon firing over the metal substructures results in an intimate micromechanical retention that is also assisted by a primary chemical adhesion.[1] As it has been clearly documented through elemental interfacial analysis studies, O links between the SiO_2 of the veneer porcelain and the oxide layer, formed by trace elements "keyed" on the surface of the metal alloy framework, to chemically join the two heterogeneous substances.[2-7] Thus, the overall bond obtained within the metal-ceramic complex attains adequate strength that has been experimentally documented and clinically confirmed.[8]

The esthetic demand to produce full coverage restorations that imitate the internal optical structure and behavior of the natural dentition, as closely as possible, led the dental industry to the development of all-ceramic systems, free of metal supporting frameworks. The brittleness of silica-based feldspathic porcelain veneers, which provide the restorations with the required depth of translucency and the necessary variety of shade options, must be mechanically supported by high-strength ceramic substructures, copings or bridge frameworks.

The efforts for the development of mechanically reinforced cores started with the high alumina porcelain in the late 1960s and continued through the '80s and '90s with the introduction of glass-infiltrated sintered ceramics and glass-ceramics. Along with the turn of the century, the development of the all-ceramic technology entered the era of densely sintered ceramics of alumina first and zirconia soon after.[9] The application of these industrially produced high-strength materials became possible though the advances of digital technology and the introduction of CAD/CAM procedures in the dental laboratories.

The combination of these core materials, with the appropriate veneering porcelains, was aimed mainly at the development of all-ceramic systems possessing improved mechanical and optical behavior properties. However, the combination of these two potentially – more or less – heterogeneous materials has not been examined in depth, especially not on the grounds of the interface created during firing of the one over the other.

It has been assumed that in the ceramic substructures containing glass (high alumina porcelain and various glass-infiltrated sintered ceramics) bearing ceramic veneers as well as in the glass-ceramics, the common silica phase present in both the core and the veneer parts defines a chemically uniform cohesive interfacial transition. In the densely sintered alumina and zirconia cores, such a unifying phase is absent and thus a chemically uniform transition does not exist.

Generally, adequate bond strength is clinically performed more or less equally by all systems.[9] Nevertheless, a detailed elemental characterization of the interfaces that develop upon firing the

appropriate veneering porcelains over the various ceramic substrates does not exist in the dental literature, or for the glass-infiltrated and glass-ceramics or for the densely sintered alumina and zirconia core complexes.

The aim of the present study was to characterize the interface comprehensively of the historically developed early and current ceramic systems applied in fixed prosthodontics like glass-ceramic, glass-infiltrated and densely sintered all-ceramic cores bearing the pertinent veneering porcelains. The null hypothesis was that elemental gradients like those reported for metal ceramic systems are involved in porcelain veneer bonding to all-ceramic core materials.

Materials and methods

In order to accumulate an integrated comparative knowledge concerning the interface under examination, 11 different brands of all-ceramic systems (reinforced core-veneer combinations), early and current, were examined. Based on the nature of the core, the systems were examined, and divided in three type-groups: glass-ceramics, glass-infiltrated ceramics, and densely sintered ceramics. The materials used in the study are presented in Table 1. Sets of three samples were fabricated (10 × 10 × 3 mm) for each ceramic system. The cores were constructed according to the indicated method and they were covered accordingly by a compatible veneer porcelain.

For the glass-ceramic group, wax patterns (10 × 10 × 3 mm) were invested in order to produce the heat-pressed glass-ceramic cores (CER, EM1, EM2, EMX, FIN). The pressing procedures took place in the pertinent for each product furnace, according to the manufacturers' instructions. The veneering procedures were followed by applying a compatible for each core glass-ceramic veneering product. For the glass-infiltrated group, prefabricated cubes (10 × 12 × 15 mm) of sintered, but not glass-infiltrated ceramics, industrially manufactured for copy-milling procedures, were used. The cubes were sliced with a thin diamond-separating disk to produce samples of 3 mm in thickness. After glass infiltration and sandblasting (50 μm/1.5 bar) the corresponding veneer of feldspathic porcelain was layered over the samples and fired accordingly. The group of densely sintered ceramics involved two subgroups. The first subgroup consisted of densely sintered alumina (PRO) and zirconia (CEC). The core samples (10 × 10 × 3 mm) were provided directly from the manufacturers. After sandblasting (Al_2O_3 50 μm/3 bar for PRO and Al_2O_3 50 μm/1.5 bar for CEC), the core samples received the appropriate veneering feldspathic porcelain build-up and were fired accordingly. The second subgroup involved densely sintered zirconia samples produced from by CAD/CAM procedures. Following sandblasting (Al_2O_3 50 μm/1.5 bar) the core samples were covered with wax (3 mm). After investing and wax burnout they then received heat-pressed glass-ceramic veneers (ZPR and ZNP).

The specimens produced for each testing group were embedded with the longest edge placed vertically in epoxy resin (Caldofix, Struers), exposing the interfacial side on the surface. The ex-

Table 1 The ceramic materials used in the study.

Product	Code	Core/veneer materials	Manufacturer
A. Glass-ceramics			
Cergo	CEG	Core: Ingot Cergo Gold pressable/ B1 Veneer: Ducera Gold DB2	Degudent Dental
IPS Empress	EM1	Core: Ingot 110/A1 dentin/body Veneer: Impulse-Incisal	Ivoclar Vivadent
IPS Empress 2	EM2	Core: Ingot 100/Layering technique Veneer: Incisal 3	Ivoclar Vivadent
IPS e.max press/ ceram	EMX	Core: Ingot IPS e.max press A3.5 Veneer: IPS e.max ceram C2	Ivoclar Vivadent
Finesse	FIN	Core: Ingot Finesse Pressable/C4 Veneer: Finesse LF	Dentsply-Ceramco
B. Glass-infiltrated ceramics			
Celay alumina	CLA	Core: In Ceram Alumina AC-12 Glass: Glass powder Al 2 Veneer: Vitadur A dentin D3	VITA Zahnfabric
Celay zirconia	CLZ	Core: In Ceram Zirconia ZC-12 Glass: Glass powder Z21 Veneer: Vitadur A dentin D3	VITA Zahnfabric
C. Densely sintered ceramics			
Cercon	CEC	Core: Cercon base Liner: Cercon porcelain S Liner Veneer: Cercon porcelain S Dentin	Degudent Dental
Veneered Procera Alumina	PRO	Core: Code No 89032.2, 89032.3, 89032.7, 89032.8, Liner: Creation Av/Liner SH-14 Veneer: Creation Av/dentin C3	Core: Nobel Biocare Veneer: Creation Willi Geller
IPS e.max ZirCad/ ZirPress	ZPR	Core: e.max ZirCAD Veneer: e.max ZirPress	Ivoclar Vivadent
Noritake Zirconia/ CZR-Press	ZNP	Core: Noritake Zirconia Veneer: CZR-Press	Kuraray Noritake Dental

Table 2 The elemental composition of core and veneer materials (wt%, means of 3 measurements).

Code	Core material	Veneer material
A. Glass-ceramics		
CEG	O: 31.18, Na: 7.38, Al: 14.54, Si: 36.17, K: 10.72	O: 30.96, Na: 8.02, Al: 9.86, Si: 36.08, K: 12.08
EM1	O: 30.49, Na: 3.83, Al: 14.51, Si: 35.24, K: 13.02, Ca: 1.67, Ti: 1.67, Ce: 0.88	O: 30.52, Na: 5.22, Al: 11.83, Si: 36.72, K: 13.53,Ca: 1.09, Ba: 0.56, Ti: 0.16, Ce: 0.37
EM2	O: 38.98, Na: 4.96, Mg: 0.58, Al: 1.35, Si: 42.85, P: 3.00, K: 4.19, Zn: 4.08	O: 32.44, Na: 6.46, Mg: 0.30, Al: 8.11, Si: 37.33, P: 0.61, K: 7.58, Ca: 1.54, Ti: 1.62, Ce: 1.78, Zn: 2.24
EMX	O: 51.82, Na: 0.25, Mg: 0.72, Al: 0.96, Si: 36.84, P: 1.87, K: 3.09, Ce: 1.48, Zn: 2.96	O: 43.85, F: 0.64, Na: 5.12, Mg: 0.15, Al: 5.80, Si: 33.42, P: 0.53, K: 5.90, Ce: 1.44, Ti: 0.77, Ce: 0.61, Zn: 1.76
FIN	O: 29.51, Na: 5.16, Al: 9.91, Si: 39.58, K: 12.15, Ca: 1.91, Ba: 1.59	O: 30.46, Na: 7.59, Mg: 3.17, Al: 5.70, Si: 38.14, K: 10.03, Ca: 2.13, Tb: 2.78
B. Glass-infiltrated ceramics		
CLA	O: 28.41, Al: 58.20, Si: 2.60, Ca: 0.57, Ti: 0.65, La: 9.57	O: 31.79, Na: 3.67, Al: 10.15, Si: 42.47, K: 9.84, Ca: 2.07
CLZ	O: 28.93, Al: 39.98, Si: 2.26, Zr: 19,96, Ca: 1.08, La: 4.74, Ce: 3.25	O: 34.34, Na: 4.13, Al: 10.49, Si: 40.55, K: 8.57, Ca: 1.73, Fe: 0.19
C. Densely sintered ceramics		
CEC	O: 11.91, Hf: 2.61, Y: 9.43, Zr: 76.05	O: 29.67, Na: 5.98, Al: 7.74, Si: 41.53, K: 10.38, Sb: 2.24, Ca :0.98, Ba: 1.48
PRO	O: 33.59, Al: 66.41	O: 34.10, Na: 5.30, Mg: 0.76, Al: 8.16, Si: 43.90, K: 6.05, Ca: 1.21,Ti: 0.51
ZPR	O: 26.42, Hf: 2.16, Y: 7.74, Zr: 63.68	O: 46.72, Na: 7.28, Al: 7.92, Si: 27.60, Zr: 1.33, K: 5.11 Ca: 1.67, Ti: 0.78, Ce: 0.77, Zn: 0.81
ZNP	O: 28.67, Al: 0.2, Hf: 2.45, Y: 2.36, P: 1.81, Zr: 64.51	O: 48.44, Na: 3.69, Mg: 0.43, Al: 8.89, Si: 29.70, K: 7.49 Ca: 0.60, Ce: 0.76

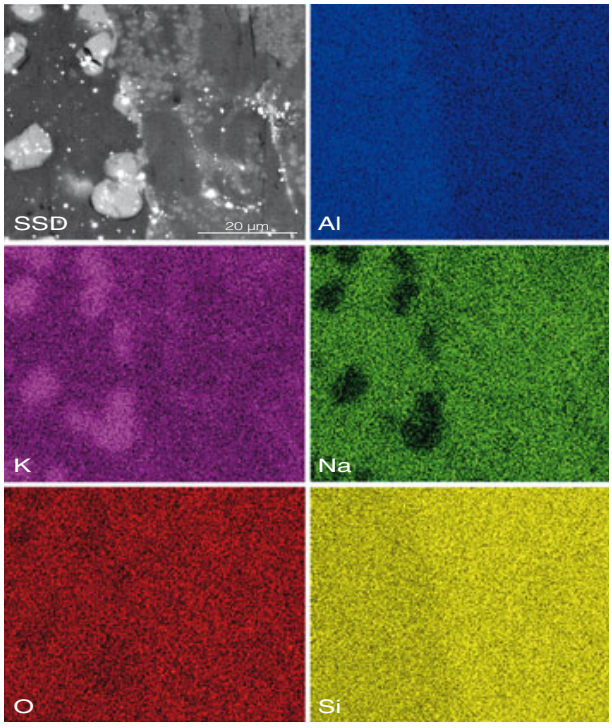

Fig 1 Backscattered electron image (SSD) of CEG core-veneer interface and the corresponding elemental maps of Al, K, Na, O and Si (2,000×, bar: 20 µm).

posed cross-section was ground by using SiC papers (220 to 2,200 grit-size) under water-cooling, then metallographically polished with diamond pastes (3, 1 and 0.25 µm, DP-Paste, Struers) in a grinding/polishing machine (Ecomet III, Buehler) and finally ultrasonically cleaned for 5 min in ethanol.

All the specimens were then sputter-coated with carbon in a sputter-coating unit (SCD 004 Sputter Coater with OCD 30 attachment, Bal-Tec) and examined in a scanning electron microscope (Quanta 200 SEM, FEI) coupled with an x-ray energy dispersive spectrometer (EDX), equipped with a super ultra-thin Be window Si(Li) detector (Sapphire CDU, Edax). The specimens had images taken at the interface by a solid-state atomic number contrast backscattered detector (SSD), to identify phases with differences in the mean atomic number ($Z > 1$). The elemental composition of the core and layer components and their interfacial elemental distributions were then determined by EDX microanalysis. Area scan analysis, multi-element area mapping and line scan analysis were used respectively. All specimens were analyzed under high vacuum (10^{-4} Pa), 25 kV accelerating voltage, 110 µA beam current 2,000× magnification, 200 s live acquisition time, 34% detector dead time and 133 eV resolution. For the elemental analysis of the core and veneer materials a sampling window of 50 x 50 µm was used. For line scan analysis, a region extending 30 µm each side the interface was studied. Quantitative analysis was performed in standardless mode, employing ZAF (Z: atomic number, A: absorption, F: fluorescence) and C-coating corrections using Genesis 5.2 software (Edax). The latter correction was employed to compensate for the absorption of the low energy x-rays of light elements.

Results

The results of the elemental analysis of the core and veneer materials are summarized in Table 2. For the group of the

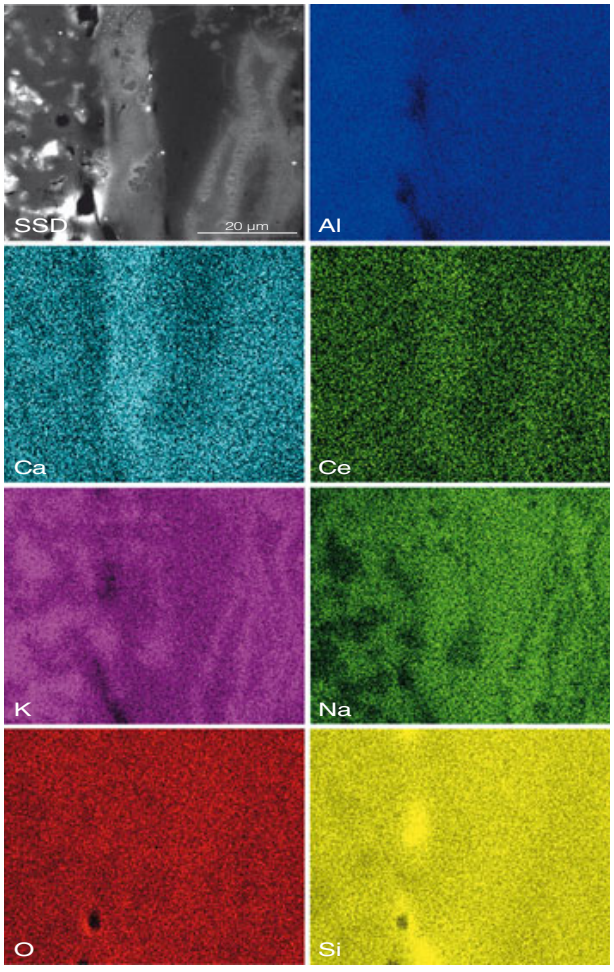

Fig 2 Backscattered electron image (SSD) of EM1 core–veneer interface and the corresponding elemental maps of Al, Ca, Ce, K, Na, O and Si (2,000×, bar: 20 µm).

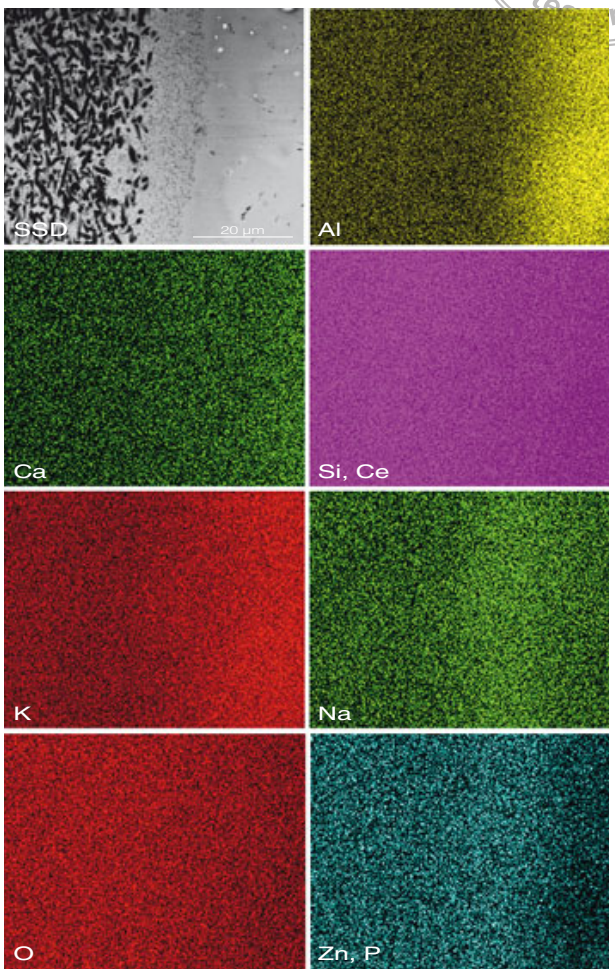

Fig 3 Backscattered electron image (SSD) of EM2 core–veneer interface and the corresponding elemental maps of Al, Ca, Ce, Si, K, Na, O, Zn and P (2,000×, bar: 20 µm).

glass-ceramics, the qualitative differences between core and veneer materials were limited to the addition of some elements (ie. Na, Mg, Ca, Ce apparently in their oxide form), in the veneer material to improve bonding with core and enhance optical characteristics. For the glass-infiltrated ceramic, the core glass component was based on a rare earth (Ce, La) containing glass, whereas the veneer component was a conventional glass. Finally the composition of the highly sintered ceramics was completely different from the veneer material, since the former mainly lack a glass phase.

Compositional backscattered electron images and representative elemental x-ray area mappings and line scans of the glass-ceramic materials are shown in Figs 1 to 5. CEG demonstrated a diffuse distribution pattern of Si, Al, and O at the interfacial region

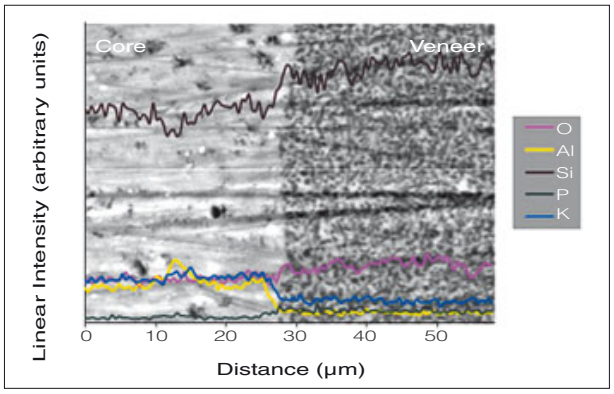

Fig 4 Backscattered electron image (SSD) of EMX core–veneer interface and the corresponding elemental line scan analysis for O, Al, Si, P, and K (2,000×).

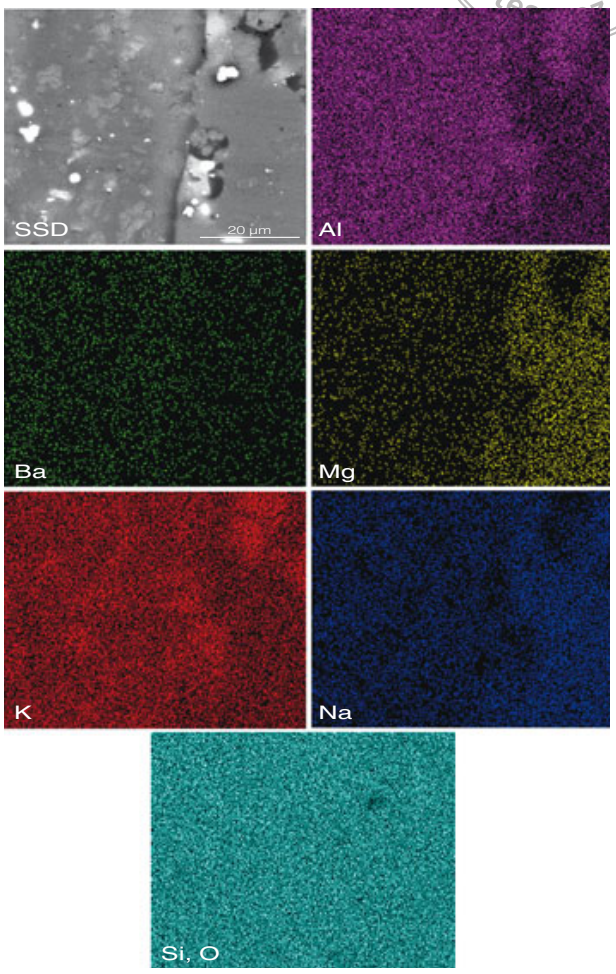

Fig 5 Backscattered electron image (SSD) of FIN core–veneer interface and the corresponding elemental maps of Al, Ba, Mg, K, Na, Si and O (2,000×, bar: 20 µm).

(Fig 1). The core presented increased Al content with islands rich in K. The distributions of K and Na were complementary, extending to each side the interface. EM1 exhibited a well-defined interfacial zone of ~10 µm thickness, facing the core material (Fig 2). This zone was rich in Ca, Ce and Si. Porosity was identified between the core surface and the bottom of the interfacial zone. Apart from this zone, the distributions of Al, O and Si were uniform along the interface, whereas Na and K illustrated a complementary structure. The needle-like structures of lithium disilicate of EM2 (Fig 3) denote the core material. As Li has a very low atomic number (Z: 3), it was not detectable by the EDX system used. On top of the disilicate structure, a transitional zone was formed with two regions, an internal granular region and an external amorphous region, occupy-

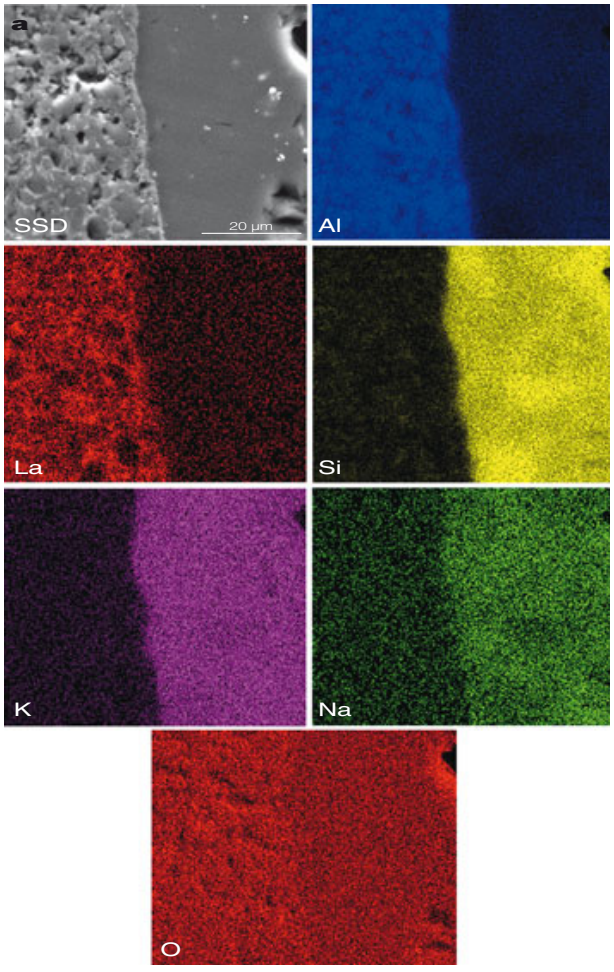

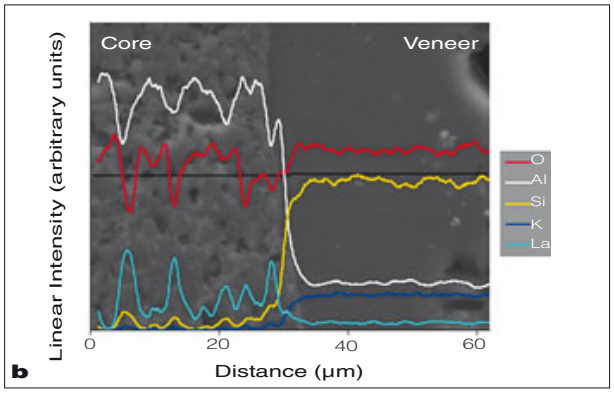

Fig 6 CLA core–veneer interfaces (2,000×). **(a)** Backscattered electron image (SSD) and the corresponding elemental maps of Al, La, Si, K, Na and O (bar: 20 µm). **(b)** Backscattered electron image (SSD) and the corresponding elemental line scan analysis for Al, O, Si, K, and La.

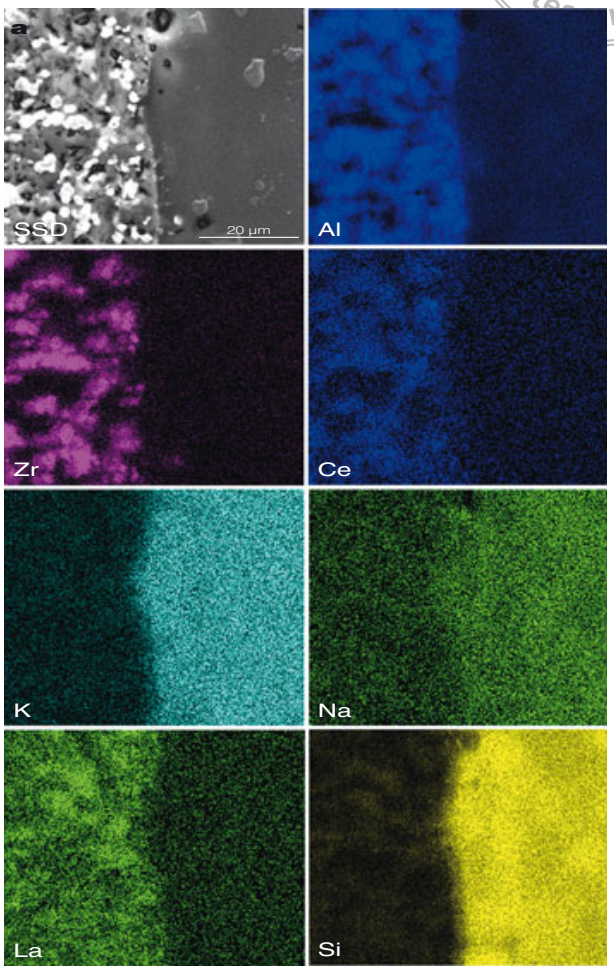

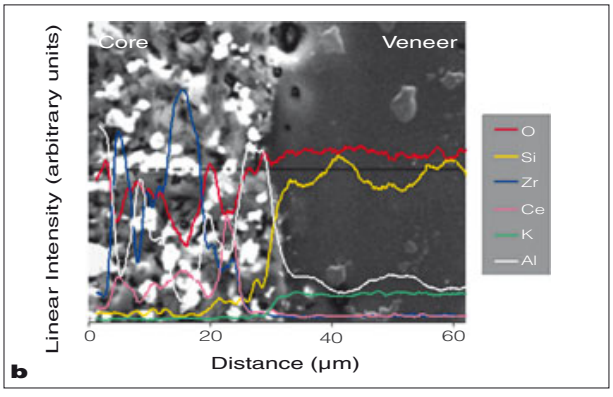

Fig 7 CLZ core–veneer interfaces (2,000×). **(a)** Backscattered electron image (SSD) and the corresponding elemental maps of Al, Zr, Ce, K, Na, La and Si (bar: 20 µm). **(b)** Backscattered electron image (SSD) and the corresponding elemental line scan analysis for O, Si, Zr, Ce, K, and Al.

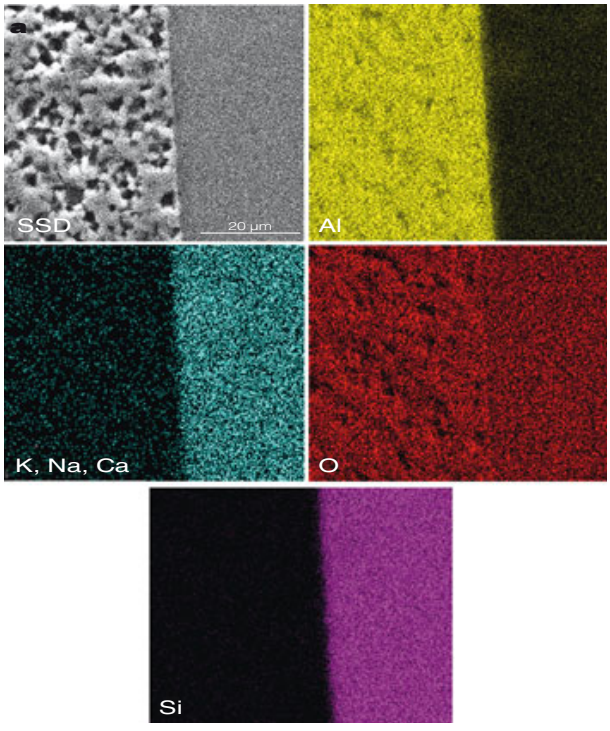

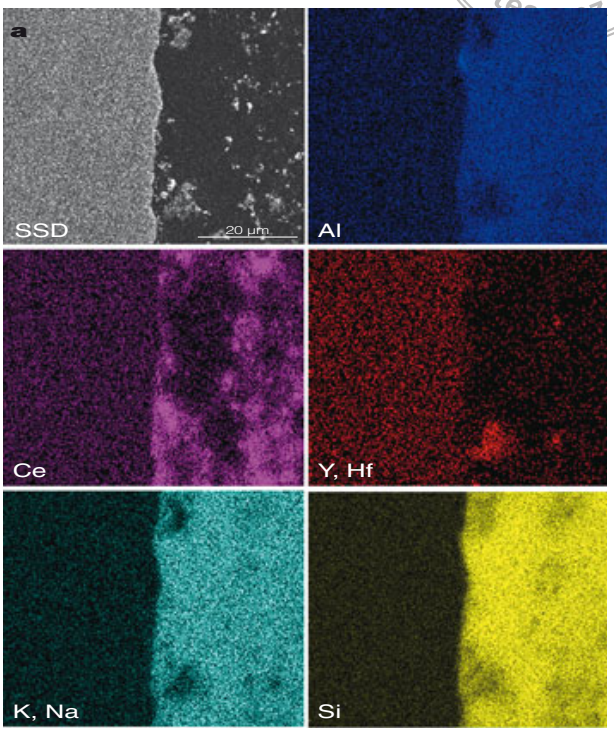

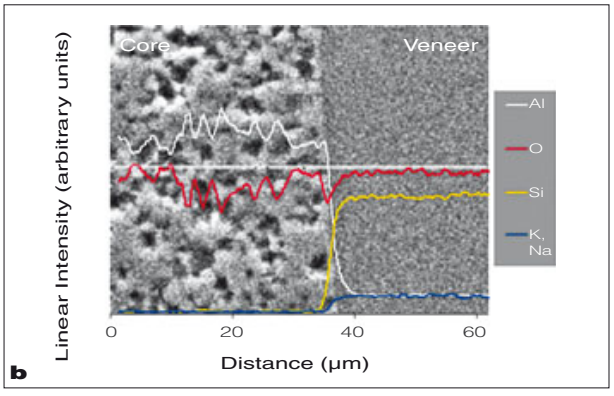

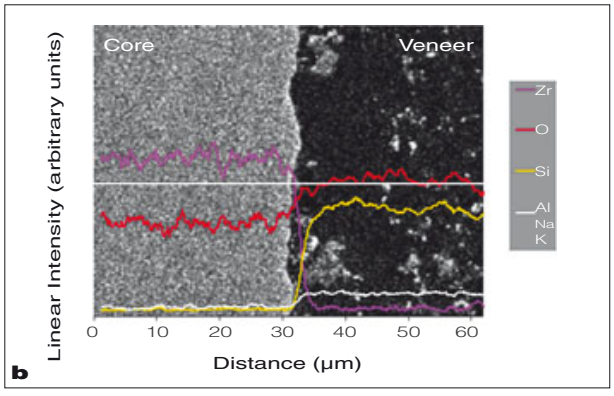

Fig 8 PRO core–veneer interfaces (2,000×). **(a)** Backscattered electron image (SSD) and the corresponding elemental maps of Al, K, Na, Ca, O and Si (bar: 20 µm). **(b)** Backscattered electron image (SSD) and the corresponding elemental line scan analysis for Al, O, Si, K, and Na.

Fig 9 CER core–veneer interfaces (2,000×). **(a)** Backscattered electron image (SSD) and the corresponding elemental maps of Al, Ce, Y, Hf, K, Na, Si, O and Zr (bar: 20 µm). **(b)** Backscattered electron image (SSD) and the corresponding elemental line scan analysis for Zr, O, Si, Al, K, and Na.

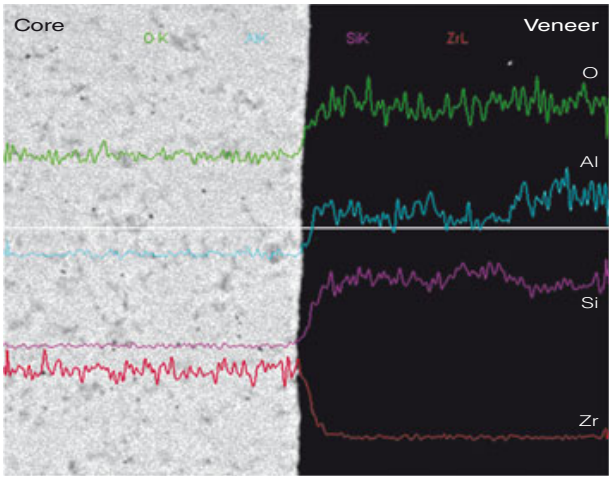

Fig 10 Backscattered electron image (SSD) of ZPR core–veneer interface and the corresponding elemental line scan analysis for O, Al, Si, and Zr (2,000×).

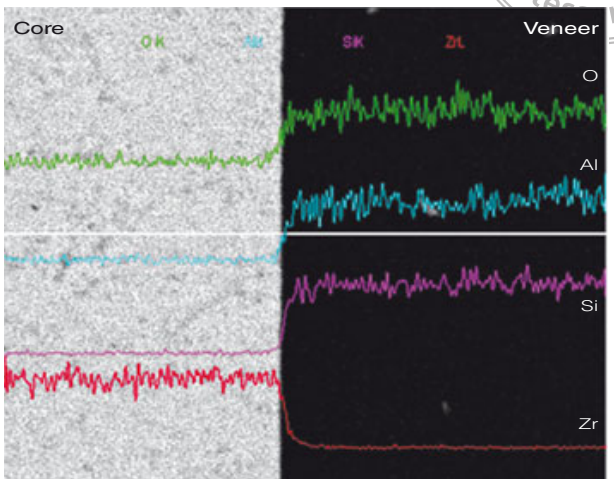

Fig 11 Backscattered electron image (SSD) of ZNP core–veneer interface and the corresponding elemental line scan analysis for O, Al, Si, and Zr (2,000×).

ing approximately ~15 μm in thickness. This zone was rich in Na, Zn and P. The Al mapping resembled the outline of the veneering material. O and Si demonstrated a rather uniform distribution, with a slightly higher content in the core material and transitional zones, while Ca and K showed an inverse profile, with slightly higher concentrations in the veneer. For EMX (Fig 4) the interfacial characteristics were similar to EM2. At the interface there was increased Si and O concentration relative to Al and P. The FIN interface (Fig 5) manifested a uniform distribution of O and Si with Al, K, Ba and Mg, Na allocated at the core and veneer locations respectively. The distribution of the latter group of elements was complementary to the first.

For the glass-infiltrated ceramic CLA, La from the alumina core and Si, Na from veneer materials showed interdiffusion zones across the interface (Figs 6a and 6b). The distribution of La was complementary to Al. O existed at both sites of the interface with reduced intensity in the veneering porcelain. For CLZ, Ce and La showed a complementary distribution to Zr and Al of the core material and extended beyond the interface into the veneer structure (Figs 7a and 7b). Moreover, the main elements of the veneer (Si, Na, K) exhibited well-defined distributions into core material, with a predominant effect of that of Na (Fig 7a). Some pores were identified at the interface.

The densely sintered ceramics demonstrated a completely different elemental distribution at the core–veneer interface. In all the materials tested, an abrupt drop of the core and veneer elements occurred at the interface, with no evidence of ionic migration or ionic interdiffusion (Figs 8 to 11). The only element with a distribution each side the interface was O.

Discussion

It has been well documented that the intraoral performance of ceramic restorations depends mainly on the location, distribution and density of critical structural defects, such as cracks and pores, which reduce material strength and contribute to failure.[10,11]

Factors like shape, thickness, loading conditions and direction, and residual stresses developed during firing and polishing may greatly contribute to the material deterioration.[12] For ceramic core materials veneered with porcelain, the structure of the interface sets an additional important parameter. The nature of bonding at the interfaces, differences in the coefficients of thermal expansion and elastic moduli accumulate interfacial stresses that may affect interlayer strength and durability.[13,14]

In the systems tested, the interface between the core and veneer materials demonstrated in most cases a clear transitional line, with limited transitional phases. The interfaces were continuous, although in some cases porosity was identified.

For glass-ceramic systems, both the core and veneer materials contained a glass phase. During porcelain firing, intermixing of the glass phase of the veneer material with that of the core may occur, due to the diffusion gradients formed in the low melting point oxides, thus creating a continuous interface. Such mechanisms may apply for CEG and FIN. For EM1, though, a distinct interphase has been identified on top of the core surface, rich in Ca, Ce, and Na. The oxides of these elements decrease the SiO_2 fusion temperature, while some (ie, Ce_2O_3, BaO, ZnO) contribute to interfacial bonding, as experienced with metal substrates.[15] A similar type of interphase, but no as clear as in EM1, was found in EM2. This was located on top of the lithium disilicate structure, with increased Na and Zn content. Careful observation of the atomic number contrast grayscale level revealed the presence of two interphases over the lithium disilicate structure: a microgranular phase in contact with the disilicate structure and on top of that a phase with a lower atomic number than the veneer. The microgranular structure may be appended to a hybrid structure of lithium disilicate. The distributions of Na and Zn corresponded to the low atomic number phase, implying a critical role of Na and Zn in interfacial bonding. For EMX, no such clear interphases were formed. Instead, increased Si and O were traced near the interface, apparently from segregation of the reactive glass during firing.

The same glass interdiffusion process seems to be implicated with the phenomena occurring at the interface of the glass-infiltrated core with the veneer material. Ce and La from core and Si and Na from veneer established elemental gradients each side the interface, while the core elements Al in CLA and Zr in CLZ showed an abrupt drop at the interface. In CLZ, Al was identified in core and veneer materials, being a component of both ceramic to provide a reinforcing effect. Lanthanum oxide containing silica/alumina glasses are hard materials with high elastic moduli, durability in alkali media and high glass transition temperatures. These properties are attributed to the higher field

strength of La than conventional alkali glass modifiers.[16] The extent to which lanthanum oxide contributes to core/veneer interfacial interactions is unknown. For the reaction mode of Ce_2O_3 (ceria) in the Ce_2O_3-SiO_2-ZrO_2 system it has been shown that is influenced by many parameters. The ability of ceria to form non-stoichiometric solid solutions may vary accordingly, resulting in different chemical compounds.[17]

For the densely sintered polycrystalline core materials, no evidence of elemental migration was identified. The results for zirconia are in agreement with recent findings.[18] It is most possible that the bonding mechanism in these materials is limited to excellent core wetting by the veneer porcelain melt and development of compressive stresses from the tailored mismatch in the coefficients of thermal expansion during cooling. For zirconia frameworks, an additional mechanism may exist; the minimal dissolution of ZrO_2 particles at grain boundaries, a procedure that is assisted by the aggressive solubility of silicate glasses towards refractory materials at moderately elevated temperatures.[19,20] Nevertheless, the latter may destabilize the tetragonal zirconia phase,[21] initiating the low temperature degradation mechanism of zirconia.[22] Although zirconia is considered as a very tough core material, it has been postulated that a better bonding occurs between glass-ceramic and veneering ceramic materials than zirconia and veneering ceramic.[23] The lack of primary chemical bonding between zirconia cores and veneering porcelain may contribute to this finding.

Conclusions

Based on the results of the present study, glass-ceramic and glass-infiltrated ceramic cores demonstrated elemental interdiffusion phenomena at the interfaces with veneering porcelain, which support the formation of primary chemical bonding. However, no such phenomena were probed between densely sintered ceramic cores and veneering porcelain. Therefore the null hypothesis was partially rejected for densely sintered polycrystalline structures.

References

1. Howe J. Bonding, structure, and properties of metal/ceramic interfaces: Part 1. Chemical bonding, chemical reaction, and interfacial structure. Int Mater Rev 1993;38:233–256.
2. Anusavice KJ, Horner JA, Fairhurst CW. Adherence controlling elements in ceramic-metal systems. I. Precious alloys. J Dent Res 1977;56:1045–1052.
3. Baran G. Oxidation kinetics of some Ni-Cr alloys. J Dent Res 1983;62:51–55.
4. Baran GR, Solution of Ni-Cr alloy oxides in an alkali alumino-silicate glass. Dent Mater 1988;4:354–359.
5. Cai Z, Watanabe I, Mitchell JC, Brantley WA, Okabe T. X-ray diffraction characterization of dental gold alloy-ceramic interfaces. J Mater Sci 2001;12:215–223.
6. Hegedus C, Daroczi L, Kokenyesi V, Beke DL. Comparative microstructural study of the diffusion zone between NiCr alloy and different dental ceramics. J Dent Res 2002;81:334–337.
7. Mackert, JR Jr, Ringle RD, Parry EE, Evans AL, Fairhurst CW. The relationship between oxide adherence and porcelain-metal bonding. J Dent Res 1988;67:474–478.
8. Walton TR. An up to 15-years longitudinal study of 515 metal-ceramic FPDs: Part 1. Outcome. Int J Prosthodont 2002;15:439–445.
9. Zarone F, Russo S, Sorrentino R. From porcelain-fused-to-metal to zirconia: clinical and experimental considerations. Dent Mater 2011;27:83–96.
10. Tinschert J, Natt G, Mautsch W, Augthun M, Spiekermann H. Fracture resistance of lithium disilicate-, alumina-, and zirconia- based three-unit fixed partial dentures: a laboratory study. Int J Prosthodont 2001;14:231–238.
11. Drummond JL. Ceramic behavior under different environmental and loading conditions. In: Eliades G, Eliades T, Brantley W. Watts D (eds). Dental Materials In Vivo - Aging and Related Phenomena. Chicago: Quintessence Publishing, 2003.
12. Wakabayashi K, Anusavice KJ. Crack initiation modes in bilayered alumina/porcelain disks as a function of core/veneer thickness ratio and supporting substrate stiffness. J Dent Res 2000;79:1398–1404.
13. De With G. Aspects of the fracture behavior of joints. In: Peteves SD (ed). Designing Interfaces for Technological Applications: Ceramic-Ceramic, Ceramic-Metal Joining. London: Elsevier, 1989.
14. Kelly JR. Perspectives on strength. Dent Mater 1995;11:103–110.
15. Chakmakchi M, Eliades G, Zinelis S. Bonding agents of low fusing cpTi porcelains: elemental and morphological characterization. J Prosthodont Res 2009;53:166–171.
16. Bois L, Guittet MJ, Barré N, Trocellier P, Guillopé S, Gautier M, Verdier P, Laurent Y. Aqueous alteration of lanthanum alumino-silicate glasses. J Non-Crystall Solids 2000;276:181–194.
17. Zec S, Boskovic S, Hrovat M, Kosec M. Contribution to phase equilibria in the Ce_2O_3 rich part of the Ce_2O_3–SiO_2–ZrO_2 system. J Eur Ceram Soc 2007;27:523–526.
18. Kawai Y, Uo M, Watari F. Microstructure evaluation of the interface between dental zirconia ceramics and veneering porcelain. Nano Biomedicine 2010;2:31–36.
19. Zeng L, Case ED, Crimp MA. The interfacial microstructure of zirconia and MaCor™ joined using spin-on interlayers. Mater Sci Eng 2001;A307:74–79.
20. Zeng L, Case ED, Crimp MA. Effects of a silica spin-on interlayer and heating mode on the joining of zirconia and MaCor™. Mater Sci Eng 2003;A357:67–74.
21. Tholey MJ, Berthold C, Swain MV, Thiel N. XRD^2 microdiffraction analysis of the interface between Y-TZP and veneering porcelain: role of application methods. Dent Mater 2010;26:545–552.
22. Chevalier J, Gremillard L, Deville S. Low-temperature degradation of zirconia and implications for biomedical implants. Ann Rev Mater Res 2007;37:1–32.
23. Ereifej N, Rodrigues FP, Silikas N, Watts DC. Experimental and FE shear-bonding strength at core/veneer interfaces in bilayered ceramics. Dent Mater 2011;27:590–597.